

Article

Sensing Characteristics of Tilted Long Period Fiber Gratings Inscribed by Infrared Femtosecond Laser

Jian Tang ^{1,2}, Cailing Fu ¹, Zhiyong Bai ¹ , Changrui Liao ¹ and Yiping Wang ^{1,*}

¹ Key Laboratory of Optoelectronic Devices and Systems of Ministry of Education and Guangdong Province, College of Optoelectronic Engineering, Shenzhen University, Shenzhen 518060, China; tangjian2@email.szu.edu.cn (J.T.); fucailing89@163.com (C.F.); baizhiyong@szu.edu.cn (Z.B.); cliao@szu.edu.cn (C.L.)

² Guangxi Colleges and Universities Key Laboratory of Microwave and Optical Wave-applied Technology, Guilin 541004, China

* Correspondence: ypwang@szu.edu.cn; Tel.: +86-755-2600-1649

Received: 26 July 2018; Accepted: 5 September 2018; Published: 7 September 2018



Abstract: We propose a novel tilted long period fiber grating (TLPPFG) design, inscribed using a line-by-line inscription technique and an infrared femtosecond (Fs) laser. The responses of this TLPPFG to external refractive index, temperature, torsion, and strain were systematically investigated to determine its sensing characteristics. The external refractive index (RI) was measured to be -602.86 nm/RIU at an RI of ~ 1.432 . The TLPPFG was used to accurately measure temperatures up to 450 °C with a sensitivity of 103.8 pm/°C. The torsion and strain sensitivity of the device were 48.94 nm/(rad/mm) and -0.63 pm/ $\mu\epsilon$, respectively. These results demonstrate that the proposed TLPPFG could be used as sensors in a series of application fields including high temperatures and external environments.

Keywords: femtosecond laser; TLPPFG; optical fiber sensor; sensing properties

1. Introduction

Optical fiber sensors have been widely used in a variety of fields due to several inherent advantages. They are highly sensitive, lightweight, compact, and immune to electric interference. Long period fiber gratings (LPFGs) are a promising passive optical fiber device, capable of coupling light in fiber core modes to several forward-propagating cladding modes, forming a series of attenuation bands in the transmission spectrum [1]. As reported in previous studies, LPFGs-based sensors have been developed to measure strain, pressure, and temperature [2]. Various fabrication methods have been used to inscribe LPFGs for specific sensing applications, including UV-light exposure [3,4], CO₂ laser irradiation [5,6], mechanical pressure [7–9], electric arc discharge [10–13], femtosecond laser (Fs) [14,15].

Among these, UV-light exposure is the most common. This process takes advantage of the photosensitivity of Ge-doped glass in the fiber core to induce periodic index modulation. However, LPFGs fabricated in this way are not resistant to high temperatures and exhibit serious grating degradation, even below 100 °C [14]. In addition, pretreated high-pressure hydrogen loading processes are required to enhance the grating writing efficiency. To solve this problem, Kondo et al. firstly fabricated an LPFG in a single mode fiber (SMF) using an 800 nm Fs laser and the point-by-point method without hydrogen loading [14]. In 2008, Allsop et al. successfully inscribed a series of symmetric and asymmetric LPFGs in photonic crystal fibers (PCFs) by a low-repetition femtosecond laser system with the point-by-point method [16]. However, this point-by-point method required precise alignment of the focused laser spot and fiber core when inscribing LPFGs. Further

improvements have been made to this fabrication techniques in the past decade. In 2010, Liu et al. presented a new method for fabricating LPFGs by periodically drilling holes into the photonic crystal fiber cladding using a focused infrared Fs laser [15]. Recently, Dong et al. proposed a transversal-scanning inscription method to fabricate LPFGs using an 800 nm infrared Fs laser [17]. It was determined that LPFGs fabricated with this method exhibit opposite bending characteristics compared with LPFGs inscribed with the point-by-point method.

The tilted long period fiber gratings (TLPGs) characterized with a $<90^\circ$ angle between the optical axis and grating plane have attracted significant attention in the past decade [18]. Detailed theoretical analysis has shown that TLPGs exhibit unique properties, such as the core layer guided-modes capable of coupling with a series of reverse high-order cladding modes, which did not occur in non-tilted LPFGs. Fabrication of TLPGs can be accomplished using several different techniques. In 2011, Wu et al. experimentally fabricated TLPGs with varying tilt angles using a CO₂ laser [19]. The resulting grating transmission spectral shape was complex and included several smaller peaks. This can be attributed to regularity of simultaneous refractive index modulation in the fiber core and cladding. Furthermore, due to the large spot size of the CO₂ laser, tilting effects in the grating were not obvious, leading to poor repeatability in the grating fabrication process. In 2012, Zhang et al. reported mechanical pressure-induced TLPGs in a solid core PCF [20]. However, TLPGs fabricated with this method often experience aging stability problems. In 2013, Chiavaioli et al. used the point-by-point method to produce specially-designed TLPGs [21]. However, the fabrication process required a manual rotation stage for inscribing grating planes at desired angles, which limited reproducibility and efficiency.

In this study, we report on a tilted long period fiber grating (TLPG) fabricated using an infrared Fs laser and a line-by-line inscription method. This technique has several advantages, including fabrication flexibility, high machining efficiency, and repeatability. The resulting TLPGs exhibit a high-quality transmission spectrum compared with those written by a CO₂ laser or mechanical pressure. A series of experiments were conducted to investigate the sensing performance of the proposed TLPGs, which achieved a sensitivity of -602.86 nm/RIU as the external refractive index was increased from 1.402 to 1.432. The device achieved a sensitivity of 103.8 pm/°C when the temperature increased from room temperature to a high of 450 °C. The inscribed attenuation bands were also found to be sensitive to torsion and strain. The measured twisting and strain sensitivities were 48.94 nm/(rad/mm) and -0.63 pm/ $\mu\epsilon$, respectively.

2. Tilted Long Period Fiber Grating Fabrications

A schematic diagram of the Fs laser micromachining apparatus is shown in Figure 1a. There are multiple primary components incorporated in the fabrication system. An Fs laser (Spectra-Physics) with a central wavelength of 800 nm, a pulse duration of 120 fs, and a repetition rate of 1 kHz was used to provide continuous laser machining. Optical power levels were adjusted through an attenuator, which was composed of a half-wave plate and a polarizer, as discussed in Li et al. [22]. The controllable power range varied from 0 to 4 mJ. An electronic shutter (THORLABS, SC10, Shanghai, China) was connected to a computer and used to control the light path (on/off) in real time during fabrication. The microscope objective lens used in our experiments exhibited a $20\times$ magnification and an NA value of 0.25. A 3D ultra-high precise (minimum incremental motion of 10 nm and a bi-directional repeatability of 80 nm) electric controllable translation stage (Newport XMS50, VP-25X and GTS30V, MICRO-CONTROLE Spectra-Physics S.A.S, Évry, France) was used to control axial motion in the X, Y and Z directions. A charge couple device (CCD) camera was used to monitor trace movements of the laser spot and capture the morphology of the TLPGs.

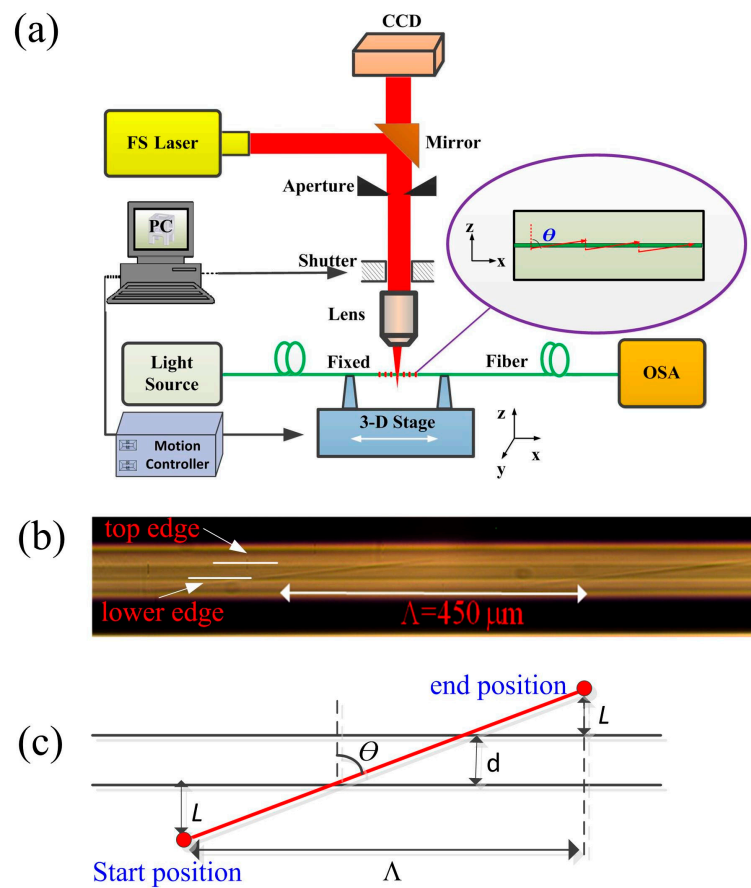


Figure 1. (a) A schematic diagram of the Fs laser micromachining apparatus; (b) An image of the TLPPFG with a grating pitch of $450 \mu\text{m}$; (c) A schematic of the Fs laser scanning trajectory.

A conventional SMF (corning) was used to fabricate the TLPPFGs in these experiments. During the fabrication process, a section of SMF coating layer was stripped off using fiber optic strippers and cleaned with ethanol. It was then fixed in place using fiber holders. One end of the SMF was connected to a broadband light source (BBS) and the other was directly attached to an optical spectrum analyzer (OSA) to monitor the evolution of the TLPPFGs transmission spectra. The laser beam was focused in the x-y plane of the fiber core with the assistance of an optical microscope (Leica DM2500, Leica Microsystems Inc., Buffalo Grove, IL, USA) and the Z translation stage. As a result, the focused laser power could effectively alter the refractive index of the fiber core without significantly affecting the cladding. Here, we define the parameter θ , which represents the angle between the movement direction of the laser spot (i.e., the tilted grating plane) and the negative Y axis. The magnitude of this angle can be calculated using the following method. Firstly, we let the laser spot be at the starting point, and the vertical distance from the lower edge of the fiber core is l . Then using soft programming, the laser spot can scan through the fiber core from the starting position to the end position with a velocity of $50 \mu\text{m/s}$. The vertical distance from the end position to the top edge of fiber core is also equal to l . The axis movement distance of the laser spot is denoted as Λ , i.e., the grating pitch. As shown in Figure 1c, we can obtain a geometric equation $\tan \theta = \Lambda / (2l + d)$, where d is the fiber diameter of $\sim 10 \mu\text{m}$. By setting scanning parameters $l = 10 \mu\text{m}$, $\Lambda = 450 \mu\text{m}$, we can obtain a value of $\theta = \arctan(450 / (2 \times 10 + 10)) = \arctan(15) \approx 86.18^\circ$. Typical laser power was set to 2.6 mW before entering the microscope objective lens. The electronic shutter was closed to obstruct the light path as the laser spot moved to the lower edge of the fiber core, to begin a new scanning cycle. This process was repeated for 30 periods, constituting a single cycle. Figure 1b shows a microscopic image taken from the top of a section of the TLPPFG.

This method was utilized to fabricate a series of TLPFGs with varying angles of 83.65° , 84.92° , 86.18° , and 88.73° , as shown in Figure 2a. All the TLPFGs were fabricated with the same period of $450\ \mu\text{m}$. The tilt angle was closely related to grating spectrum quality. During fabrication, the grating spectrum was nearly eliminated for the tilt angles below 83.65° . The dip in the resonant wavelength decreased noticeably for tilt angles above 88.73° . As such, there exists an optimal tilt angle for grating inscription. Yin et al. determined the optimal angle for TLPFGs formation to be $\sim 87^\circ$ [23], which agrees well with our experimental results. In this study, a tilt angle of 86.18° as the optimum was used for fabricating three different TLPFGs with periods of $420\ \mu\text{m}$, $440\ \mu\text{m}$, and $460\ \mu\text{m}$, as illustrated in Figure 2b, Figure 2c, and Figure 2d, respectively. Larger grating periods resulted in longer resonant wavelengths under the same laser power machining conditions. This implies the resonance wavelength exhibits a red shift an increasing grating pitch. As seen in Figure 2b, the resonance wavelength dip reached a maximum value of $-15.86\ \text{dB}$ at $1460.8\ \text{nm}$ after three scanning cycles. However, the transmission spectrum dramatically deteriorated after the fourth scanning cycle. This indicates that an over-coupling phenomenon occurred, similar to that of non-tilted LPFGs reported in ref. [24,25]. As shown in Figure 2c, the dip in the resonant wavelength around $1522.4\ \text{nm}$ can reach up to $-16.50\ \text{dB}$, which is a little smaller than TLPFGs fabricated by CO_2 laser irradiation [19]. This is because the small size ($\sim 3\ \mu\text{m}$ in diameter) of the focused femtosecond laser spot leads to relatively small refractive index modulation in the fiber core. Furthermore, Figure 2d demonstrates that our proposed method had a higher writing efficiency (less than 5 min), as high-quality TLPFGs transmission spectra were achieved with only two scanning cycles by optimizing writing parameters (laser power and scanning velocity). In order to better decide the cladding modes of the resonance wavelengths, we employed a mode field observation system similar to ref. [1] to observe the resonance wavelengths of $1552.4\ \text{nm}$ and $1605.4\ \text{nm}$, as shown in the inset of Figure 2c and d respectively.

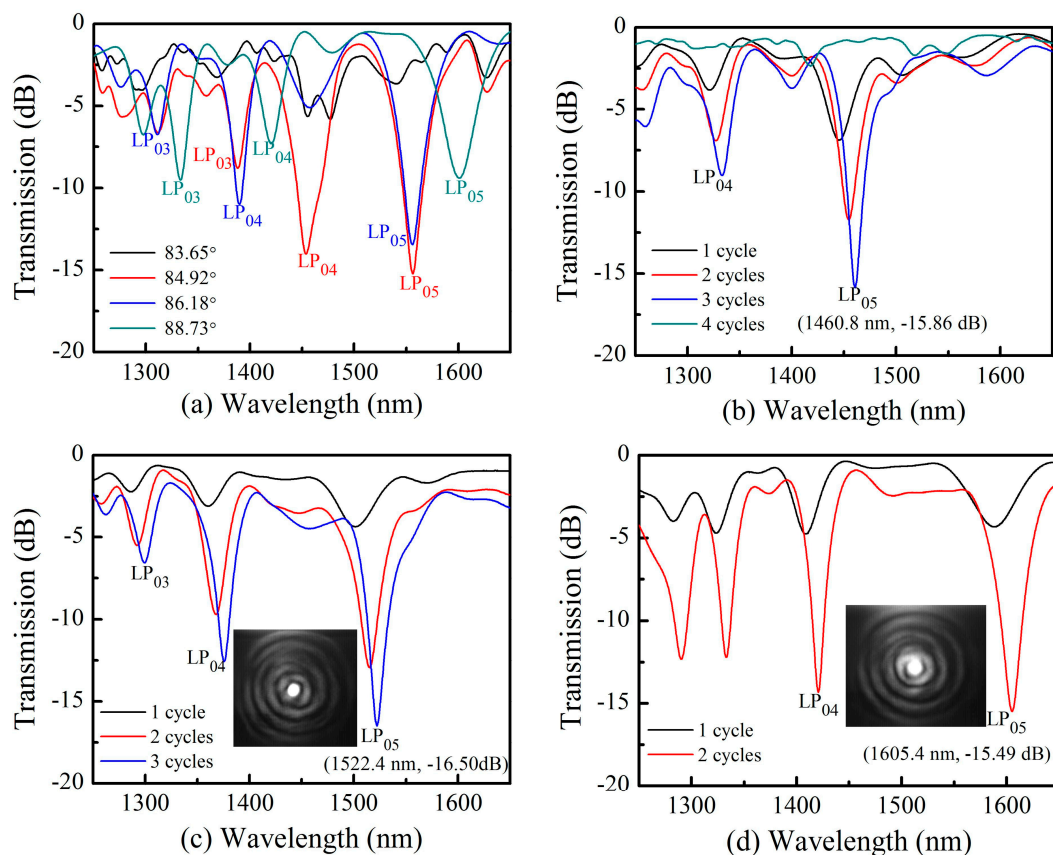


Figure 2. Various TLPFG transmission spectra, including (a) TLPFGs with varying tilted angles; (b) A TLPFG with a period of $420\ \mu\text{m}$; (c) a TLPFG with a period of $440\ \mu\text{m}$; (d) A TLPFG with a period of $460\ \mu\text{m}$.

A series of TLPFGs samples were fabricated with various grating pitches to demonstrate the repeatability of our proposed method, as shown in Figure 3. From Figure 3a we observe that variations in the resonant wavelength were within ± 2 nm, which demonstrates that the refractive index modulation was relatively uniform for each sample. The depth of the resonant dip was controllable within a fluctuation range of only ± 0.5 dB, as shown in Figure 3b. These results indicate that our proposed method has excellent repeatability and high stability during TLPFGs fabrication.

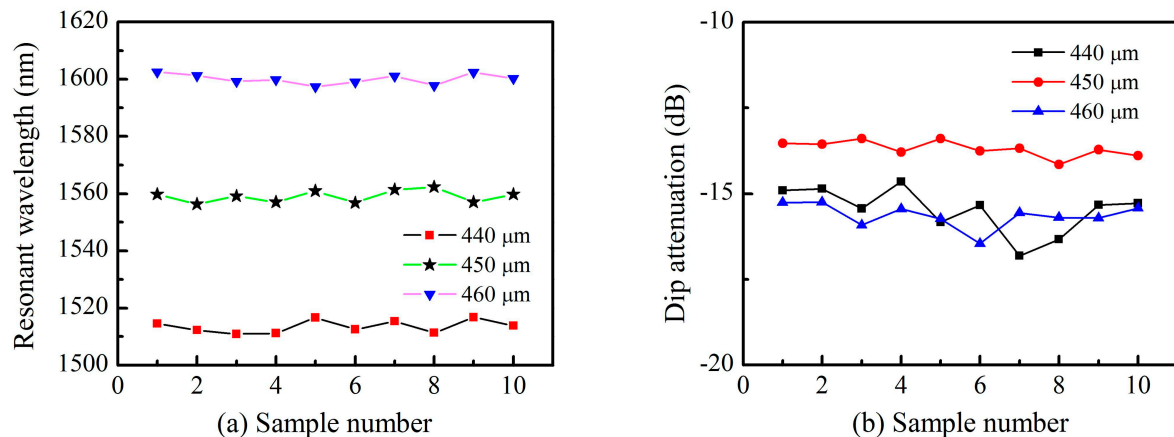


Figure 3. (a) The resonance wavelength; (b) The resonance depth of TLPFGs with different grating pitches.

3. Refractive Index Sensing Characteristic

A series of experiments were conducted to access TLPFGs optical properties. Excluding a high temperature experiment, all tests were performed at room temperature. An ASE (Fiber Lake) light source with a wavelength ranging from 1250–1650 nm and an OSA (YOKOGAWA AQ6370C) with a minimum resolution of 0.02 nm were used in the experiments. The results provide an assessment of the sensing applications of the proposed TLPFGs design.

Conventional LPFGs are sensitive to variations in refractive index. This is caused by the formation of resonance loss peaks through coupling between the core mode and several high-order cladding modes, which are highly sensitive to outer cladding mediums. As such, TLPFGs have been used as refractive index sensors in a variety of studies [26–28].

In this study, refractive index response measurements were conducted using a TLPFG with a period of 460 μm and a total of 30 periods. The grating had three distinct resonance wavelengths attributed to different high order cladding modes, coupled to the core mode in a wavelength range of 1250–1650 nm. One end of the TLPFG was fixed in a fiber clamp and the other end was attached to a 25 g small weight, providing a constant strain to align the fiber along the fiber axis direction. The grating area was completely immersed in a series of commercial refractive index matching liquids (Cargille Lab—<http://www.cargille.com>) ranging from 1.402 to 1.442. Each grating variation spectrum profile was recorded as it was in a stable state. About 5 min are required during this process.

The grating area was cleaned with ethanol after each measurement, shifting the spectrum back to its original values in air. Three resonance wavelengths were observed which exhibited different refractive index responses, as shown in Figure 4a. High-order coupled cladding modes exhibited relatively larger sensitivities. The resonance wavelength at 1559.7 nm with pattern of LP₀₅ shifted ~ 21.08 nm toward the short wavelength regime as the refractive index increased from 1.000 to 1.442. However, the low-order resonance wavelength at 1331.24 nm with a pattern of LP₀₃ only shifted ~ 1.24 nm. Figure 4b shows a magnified wavelength shift spectrum at 1599.7 nm. From this we observe the resonance wavelength includes an obvious shift while the transmission power showed almost no change. The relationship between refractive index and wavelength is shown in Figure 4c. The resonance wavelength follows a nonlinear relationship for refractive index between 1.000 and

1.442 and a linear relationship between 1.432 and 1.442. The resulting sensitivity of LP₀₅ reached -602.86 nm/RIU with a fitting degree of $R^2 = 0.997$ as shown in Figure 4d. This result is on the same order with the ultra-long period gratings inscribed using an 800 nm Fs lasers [29]. Our proposed TLPFGs exhibits a high refractive index sensitivity, compared with D-shaped fiber grating refractive index sensor induced by an 800 nm Fs laser with a sensitivity of only ~ 30 nm/RIU [30].

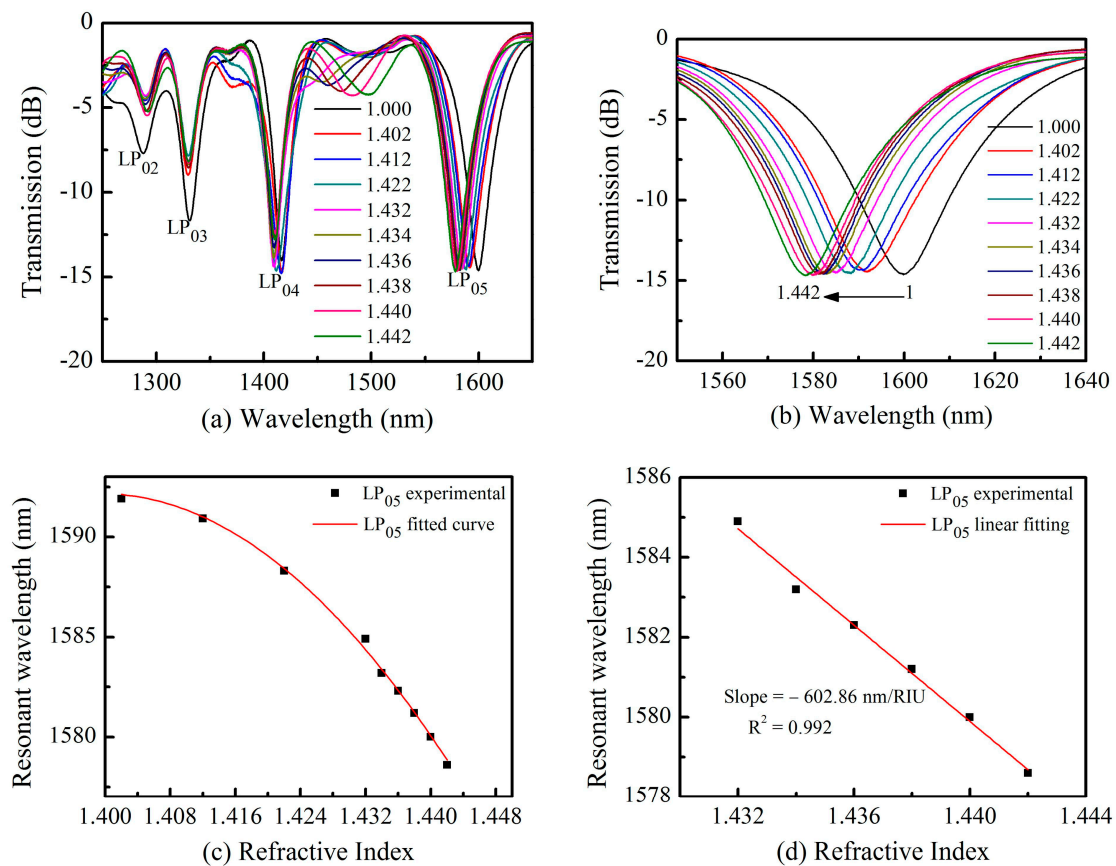


Figure 4. (a) The transmission spectrum shift of TLPFG versus the refractive index variation; (b) The magnified wavelength shift spectrum at 1599.7 nm; (c) Polynomial term fitting of resonance wavelengths as the refractive index increased from 1.400 to 1.442; (d) The Linear Fitting of resonance wavelength as the refractive index increased from 1.432 to 1.442.

4. High-Temperature Sensing Characteristic

Optical fiber sensors have played an important role in the fields of defense, aerospace, and modern industry. Several studies have investigated the high-temperature properties of LPFGs inscribed in different types of optical fibers [29,31,32]. However, the high temperature response of TLPFGs has not been studied as extensively. In this section, we performed high-temperature experiments to characterize the thermal response of TLPFGs inscribed in an SMF using an Fs laser. The TLPFGs used in these experiments had a grating pitch of $440 \mu\text{m}$ and a total of 30 periods.

The TLPFG was placed in a temperature-controlled thermoelectric oven within an accuracy of ± 1 °C, to observe thermally-induced variations in its grating spectral profile. During these measurements, the temperature was increased from room temperature (~ 25 °C) to 450 °C with a step size of 25 °C. The temperature was maintained for 10 min during each measurement to record the stabilized grating transmission spectrum using an OSA.

As shown in Figure 5a, all three resonance wavelengths in the range from 1250 to 1650 nm shifted towards longer wavelengths as the temperature increased from 25 °C to 450 °C. It is evident that the resonance loss peak of the lower-order cladding modes (LP₀₄) at 1376.3 nm decreased much faster

than the high-order cladding modes (LP₀₅) at 1511.9 nm. Lower-order resonance loss peaks exhibited wavelength shifts of 23.2 nm while high-order resonance loss peaks shifted ~32.8 nm over the same temperature range, as illustrated in Figure 5b. This indicates that high-order cladding resonance wavelength with pattern of LP₀₅ shows a relatively high temperature response sensitivity, as high as $S_1 = 103.3 \text{ pm}/^\circ\text{C}$, with good linearity ($R_1^2 = 0.983$) as shown in Figure 5c. This temperature response sensitivity is larger than many other high temperature sensors based on optical fibers [14,32]. Staying at 450 °C about 20 min, then the temperature was gradually cooled down to room temperature with a step of 25 °C. At each point, the temperature was maintained for 10 min to record the data. Linear fitting of the experimental results was conducted, achieving a fitting degree of 0.980. The slope of this fit corresponds a sensitivity of $S_2 = 98.1 \text{ pm}/^\circ\text{C}$ as shown in Figure 5c.

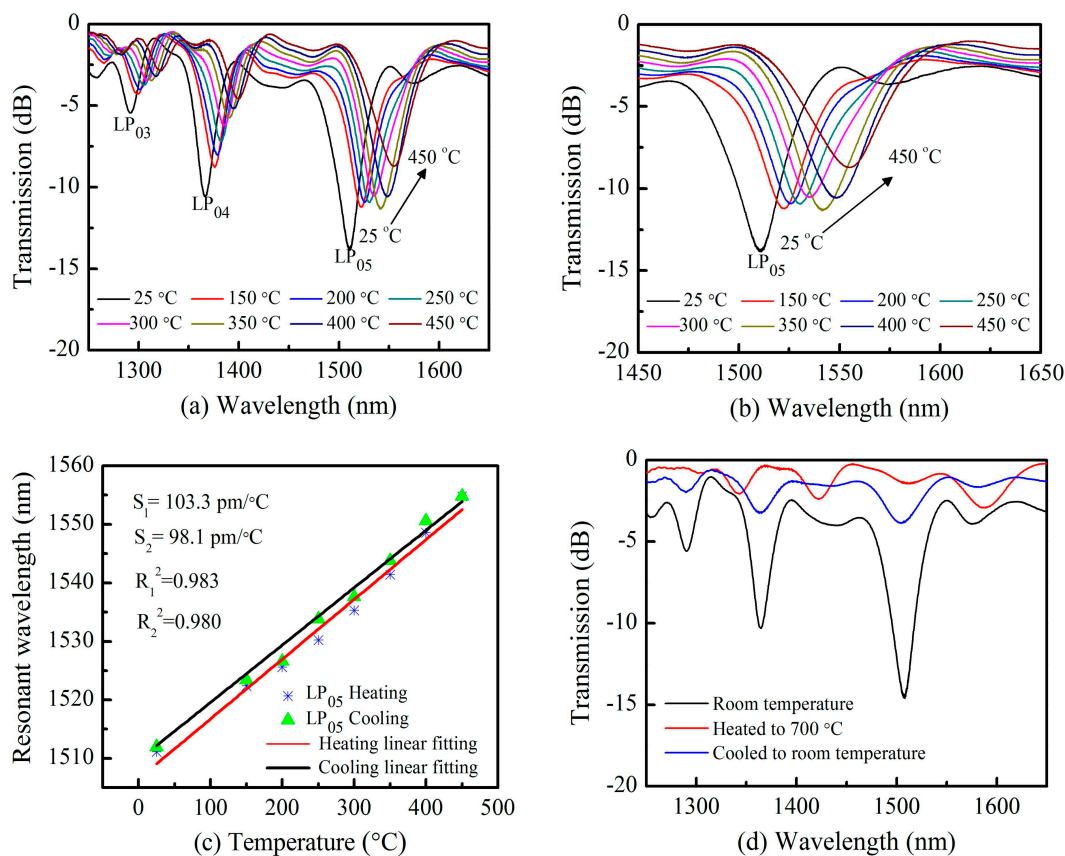


Figure 5. (a) The transmission spectrum shift of the TLPPFG versus temperature variations from 25 °C to 450 °C; (b) The resonance wavelengths shift shifts versus temperature variations from 25 °C to 450 °C; (c) Polynomial term fitting of resonance wavelength as the temperature increased to 450 °C and then cooled to 25 °C again; (d) The transmission spectrum of a TLPPFG under various temperature conditions.

Temperature endurance was further investigated by heating the TLPPFG to 700 °C and then cooling it to room temperature. Figure 5d shows variations in the transmission spectrum during this process. The grating degraded dramatically and the resonance dip disappeared entirely as the temperature approached 700 °C, indicating the TLPPFG could no longer function as an optical waveguide. The reason may be that the Fs laser-induced index change here relaxes above 700 °C as reported in reference [14]. As the TLPPFG was cooled down to room temperature, its transmission spectrum was gradually restored but the resonance dip remained in a deteriorated state, due to the effects of high temperature. It also indicates that the high temperature (>500 °C) may degrade the gratings spectra [14]. The proposed TLPPFG maintained a high-quality transmission spectrum demonstrating excellent thermal stability as the temperatures below 450 °C. In contrast, TLPPFGs fabricated with UV-light exhibit grating degradation at temperatures below 100 °C. The primary reason is that refractive index changes caused

by the focused irradiation of femtosecond pulses differ from those induced by UV-light induced [14]. As such, TLPFGs inscribed by Fs laser could be used for potential applications in the field of high temperature sensing.

5. Torsion Sensing Characteristic

Optical fiber torsion sensors have been widely used in the automotive industry and for anthropomorphic robotics applications, due to their advantages of being lightweight and immune to electronic interference [33]. Several optical-fiber-based torsion sensors have been reported in the past few years, including corrugated LPFGs, UV radiation-induced tilted fiber gratings, and Sagnac interferometers [34]. However, many of these devices cannot effectively determine the direction (clockwise or counter-clockwise) of the applied torsion, which limits their practical application. For this reason, high-sensitivity sensors have been investigated to distinguish both the torsion angle and direction simultaneously.

An experimental setup similar to that of Deng et al. [33] was used to investigate the torsion sensing properties of our proposed TLPFGs. Measurements were conducted using electronic controllable rotators which could twist the grating samples in two different rotate directions with a minimum angle of 0.1° . The distance between these two rotators (the twist length L) was equal to 55 mm in our experiments. The rotation angle was denoted as α . Thus, the applied torsion τ could be written as $\tau = \alpha/L = \alpha/0.055 \approx 18\alpha$ (rad/m). The rotation angle α was measured from $0^\circ \pm 240^\circ$ with an interval of 60° . Positive angles represented the clockwise rotation, while negative angles indicated counter-clockwise rotation. Figure 6a shows resonance wavelength shifts in the transmission spectra as the torsion τ varied from -0.076 rad/mm (-240°) to $+0.076$ rad/mm ($+240^\circ$). After each test, the spectrum was shifted back to its original values (0°). This process will cost about 2 min. It is evident that the resonance wavelength with pattern of LP_{05} (as shown in Figure 2b shows a red shift when the applied torsion is clockwise, and vice versa. Wavelength shifts are plotted in Figure 6b. An approximately linear relationship ($R^2 = 0.934$) was observed between the wavelength shift and the applied torsion during both clockwise and counterclockwise rotation. As such, a linear fitting was applied to the data. The resulting slope quantifies TLPFG torsion sensitivity, reaching a value of 48.94 nm/(rad/mm). This is twice as high as conventional non-tilted LPFGs inscribed in an SMF, with an average of ~ 23 nm/(rad/mm) [33].

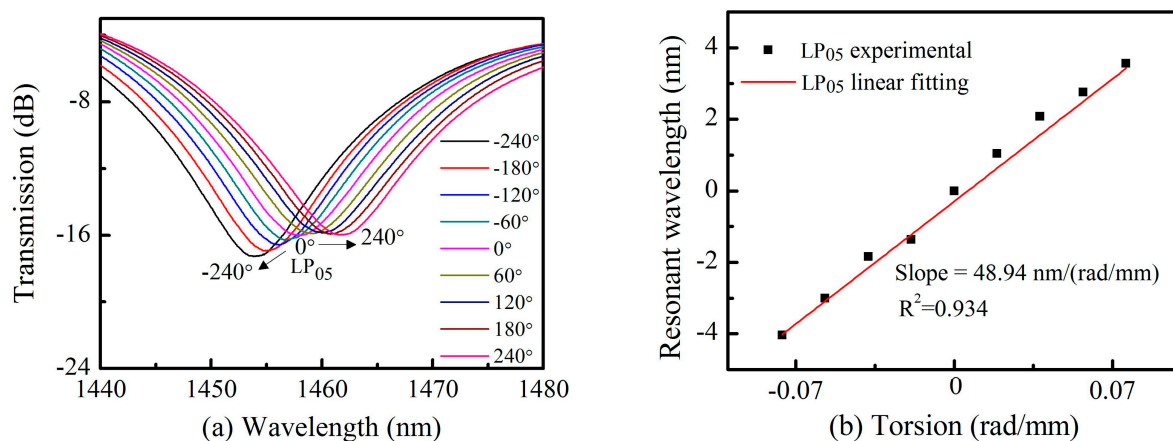


Figure 6. (a) Resonance wavelength shifts for TLPFGs under an applied torsion in the range of -0.076 rad/mm to $+0.076$ rad/mm; (b) A linear fitting between the torsion and wavelength shift.

6. Strain Sensing Characteristic

Applying strain to LPFGs along the axial direction leads to axially stretching, which causes variations in the grating pitch Λ and the refractive index of both the core and cladding, due to photo-elastic effects in the fiber. This induces resonant wavelength shifts in LPFGs, which have been

used as strain sensors in multiple studies [35]. However, the strain properties of TLPFGs have not been investigated as thoroughly. In this experiment, the employed TLPFG sample had a grating pitch of 440 μm and a total of 30 periods. It posed LP₀₅ cladding modes around the resonance dip of 1516.8 nm similar to Figure 2c.

The strain sensitivity of the proposed TLPFG was investigated, using the strain measurement setup discussed in our previous publication [36]. Two ends of the grating area were fixed by a two-micrometer translation stage with a 5 μm resolution. The distance between them was 10 cm, and the minimum strain change was $\Delta\varepsilon = 100 \mu\varepsilon$. As shown in Figure 7a, the resonance wavelength with pattern of LP₀₅ exhibited a blue shift for the applied strains ranging from 0 to 2500 $\mu\varepsilon$, as recorded by an OSA with a resolution of 0.02 nm. This implies that TLPFG can withstand a strain of 2500 $\mu\varepsilon$ without breaking. It is noted that at each test point we need about 2 min to record the stable transmission spectrum. Linear fitting of the experimental results was conducted, achieving a fitting degree of 0.995 as shown in Figure 7b. The slope of this fit corresponds a strain response of $-0.63 \text{ pm}/\mu\varepsilon$, which is higher than the sensitivity of LPFG etched in SMFs by CO₂ laser pulses ($-0.45 \text{ pm}/\mu\varepsilon$ [37]). This result support the use of TLPFGs as a strain sensor in practical applications.

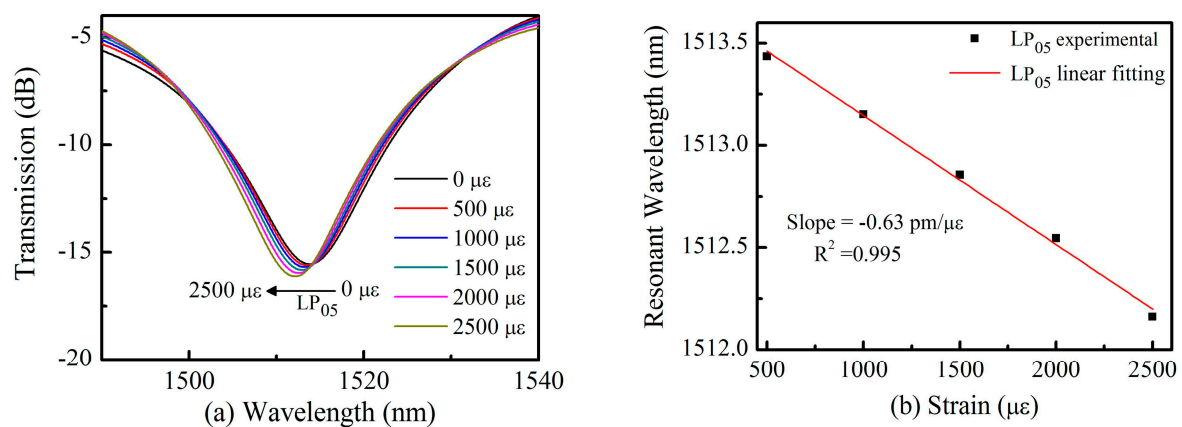


Figure 7. (a) TLPFG resonance wavelength shifts under an applied strain ranging from 0 to 2500 $\mu\varepsilon$; (b) A linear fitting between the strain and wavelength shift.

7. Conclusions

We have demonstrated a TLPFG fabrication method using an infrared femtosecond laser and a line-by-line inscription technique. The resulting TLPFG exhibited a high-quality transmission spectrum and excellent repeatability. The external refractive index, temperature, twist, and strain sensing characteristics of the TLPFG were investigated experimentally. As the surrounding refractive index gradually increased, the resonance wavelength of the TLPFG exhibits a blue shift with a sensitivity of $-602.86 \text{ nm}/\text{RIU}$ at an external RI of ~ 1.435 . The TLPFG could withstand a high temperature of up to 450 $^{\circ}\text{C}$, with a temperature sensitivity of 103.8 $\text{pm}/^{\circ}\text{C}$. It could also be used as a torsion sensor capable of determining the twisting direction. Consequently, it is anticipated that the TLPFG-based sensors could be used for a series of practical engineering applications.

Author Contributions: J.T. and C.F. performed the experiments and wrote the paper; C.L., Z.B. and Y.W. contributed to analyze data and polish the paper.

Funding: National Natural Science Foundation of China (NSFC) (grant nos. 61425007, 61605129, 61675137 and 61805155), Guangdong Natural Science Foundation (grant nos. 2015B010105007, 2015A030313541, 2014A030308007 and 2018A030310581), China Postdoctoral Science Foundation (grant nos. 2018M633115, 2017M612720 and 2016M600669), Science and Technology Innovation Commission of Shenzhen (grant nos. JCYJ20170302152718747, JCYJ20160427104925452, JCYJ20170412105604705 and JCYJ20160307143716576), Research Funding from Shenzhen University (grant no. 2016030), and Development and Reform Commission of Shenzhen Municipality Foundation.

Conflicts of Interest: The authors declare no conflict of interest. The founding sponsors had no role in the design of the study; in the collection, analyses, or interpretation of data; in the writing of the manuscript, and in the decision to publish the results.

References

1. Liu, S.; Zhang, Y.; Fu, C.; Bai, Z.; Li, Z.; Liao, C.; Wang, Y.; He, J.; Liu, Y.; Wang, Y. Temperature Insensitivity Polarization-Controlled Orbital Angular Momentum Mode Converter Based on an LPFG Induced in Four-Mode Fiber. *Sensors* **2018**, *18*, 1766. [[CrossRef](#)] [[PubMed](#)]
2. Yiping, W. Review of long period fiber gratings written by CO₂ laser. *J. Appl. Phys.* **2010**, *108*, 11.
3. Morishita, K.; Miyake, Y. Fabrication and resonance wavelengths of long-period gratings written in a pure-silica photonic crystal fiber by the glass structure change. *J. Lightwave Technol.* **2004**, *22*, 625–630. [[CrossRef](#)]
4. Guan, B.-O.; Tam, H.-Y.; LWChan, H.; Chung-Loong, C.; Demokan, M.S. Growth characteristics of long-period gratings in hydrogen-loaded fibre during and after 193 nm UV inscription. *Meas. Sci. Technol.* **2001**, *12*, 818–823. [[CrossRef](#)]
5. Wang, P.; Li, H. Helical long-period grating formed in a thinned fiber and its application to a refractometric sensor. *Appl. Opt.* **2016**, *55*, 1430–1434. [[CrossRef](#)] [[PubMed](#)]
6. Zhang, L.; Liu, Y.; Cao, X.; Wang, T. High Sensitivity Chiral Long-Period Grating Sensors Written in the Twisted Fiber. *IEEE Sens. J.* **2016**, *16*, 4253–4257. [[CrossRef](#)]
7. Joung Woo, H.; Jong Hun, L.; Joon Yong, C.; Hyun Soo, J.; Kyung Shik, L. A birefringence compensation method for mechanically induced long-period fiber gratings in optical communication and sensing systems. In Proceedings of the 2002 15th Optical Fiber Sensors Conference Technical Digest, Portland, OR, USA, 10 May 2002.
8. Savin, S.; Digonnet, M.J.F.; Kino, G.S.; Shaw, H.J. Tunable mechanically induced long-period fiber gratings. *Opt. Lett.* **2000**, *25*, 710–712. [[CrossRef](#)] [[PubMed](#)]
9. Yu, X.; Shum, P.; Ren, G.B. Highly Sensitive Photonic Crystal Fiber-Based Refractive Index Sensing Using Mechanical Long-Period Grating. *IEEE Photonics Technol. Lett.* **2008**, *20*, 1688–1690. [[CrossRef](#)]
10. Yin, G.; Wang, Y.; Liao, C.; Zhou, J.; Zhong, X.; Wang, G.; Sun, B.; He, J. Long Period Fiber Gratings Inscribed by Periodically Tapering a Fiber. *IEEE Photonics Technol. Lett.* **2014**, *26*, 698–701. [[CrossRef](#)]
11. Smietana, M.; Bock, W.J.; Mikulic, P.; Chen, J. Increasing sensitivity of arc-induced long-period gratings—pushing the fabrication technique toward its limits. *Meas. Sci. Technol.* **2011**, *22*, 015201. [[CrossRef](#)]
12. Iadicicco, A.; Campopiano, S. Sensing Features of Long Period Gratings in Hollow Core Fibers. *Sensors* **2015**, *15*, 8009–8019. [[CrossRef](#)] [[PubMed](#)]
13. Esposito, F.; Ranjan, R.; Campopiano, S.; Iadicicco, A. Experimental Study of the Refractive Index Sensitivity in Arc-induced Long Period Gratings. *IEEE Photonics J.* **2017**, *9*, 1–10. [[CrossRef](#)]
14. Kondo, Y.; Nouchi, K.; Mitsuyu, T.; Watanabe, M.; Kazansky, P.G.; Hirao, K. Fabrication of long-period fiber gratings by focused irradiation of infrared femtosecond laser pulses. *Opt. Lett.* **1999**, *24*, 646–648. [[CrossRef](#)] [[PubMed](#)]
15. Liu, S.; Jin, L.; Jin, W.; Wang, D.; Liao, C.; Wang, Y. Structural long period gratings made by drilling micro-holes in photonic crystal fibers with a femtosecond infrared laser. *Opt. Express* **2010**, *18*, 5496–5503. [[CrossRef](#)] [[PubMed](#)]
16. Allsop, T.; Kalli, K.; Zhou, K.; Lai, Y.; Smith, G.; Dubov, M.; Webb, D.J.; Bennion, I. Long period gratings written into a photonic crystal fibre by a femtosecond laser as directional bend sensors. *Opt. Commun.* **2008**, *281*, 5092–5096. [[CrossRef](#)]
17. Dong, X.-R.; Sun, X.-Y.; Li, H.-T.; Hu, Y.-W.; Duan, J.-A.; Zhou, J.-Y.; Wang, C. Femtosecond laser fabrication of long period fiber gratings by a transversal-scanning inscription method and the research of its orientational bending characteristics. *Opt. Laser Technol.* **2015**, *71*, 68–72. [[CrossRef](#)]
18. Wu, R.; Liu, Y.; Chen, N.; Pang, F.; Wang, T. Fabrication and Sensing Characteristics of Tilted Long-Period Fiber Gratings. In Proceedings of the Advanced Sensor Systems and Applications V, Beijing, China, 5–7 November 2012.

19. Rui, W.; Yunqi, L.; Jian, Z.; Na, C.; Fufei, P.; Tingyun, W. Fabrication of tilted long-period fiber gratings by CO₂ laser. In Proceedings of the Asia Communications and Photonics Conference and Exhibition 2011, Shanghai, China, 13–16 November 2011.
20. Zhang, Y.F.; Chan, C.C.; Chan, Y.M.; Zu, P. Tilted Long Period Gratings Pressure Sensing in Solid Core Photonic Crystal Fibers. *IEEE Sens. J.* **2012**, *12*, 954–957. [[CrossRef](#)]
21. Chiavaioli, F.; Trono, C.; Baldini, F. Specially designed long period grating with internal geometric bending for enhanced refractive index sensitivity. *Appl. Phys. Lett.* **2013**, *102*, 231109. [[CrossRef](#)]
22. Li, Z.; Liao, C.; Chen, D.; Song, J.; Jin, W.; Peng, G.-D.; Zhu, F.; Wang, Y.; He, J.; Wang, Y. Label-free detection of bovine serum albumin based on an in-fiber Mach-Zehnder interferometric biosensor. *Opt. Express* **2017**, *25*, 17105–17113. [[CrossRef](#)] [[PubMed](#)]
23. Yin, G.; Lou, S.; Li, Q.; Zou, H. Theory analysis of mode coupling in tilted long period fiber grating based on the full vector complex coupled mode theory. *Opt. Laser Technol.* **2013**, *48*, 60–66. [[CrossRef](#)]
24. Vengsarkar, A.M.; Lemaire, P.J.; Judkins, J.B.; Bhatia, V.; Erdogan, T.; Sipe, J.E. Long-period fiber gratings as band-rejection filters. *J. Lightwave Technol.* **1996**, *14*, 58–65. [[CrossRef](#)]
25. Erdogan, T. Fiber grating spectra. *J. Lightwave Technol.* **1997**, *15*, 1277–1294. [[CrossRef](#)]
26. Hu, D.J.J.; Lim, J.L.; Jiang, M.; Wang, Y.; Luan, F.; Shum, P.P.; Wei, H.; Tong, W. Long period grating cascaded to photonic crystal fiber modal interferometer for simultaneous measurement of temperature and refractive index. *Opt. Lett.* **2012**, *37*, 2283–2285. [[PubMed](#)]
27. Guan, C.; Tian, X.; Li, S.; Zhong, X.; Shi, J.; Yuan, L. Long period fiber grating and high sensitivity refractive index sensor based on hollow eccentric optical fiber. *Sens. Actuators B Chem.* **2013**, *188*, 768–771. [[CrossRef](#)]
28. Chong, J.H.; Shum, P.; Haryono, H.; Yohana, A.M.; Lu, K.; Zhu, Y. Measurements of refractive index sensitivity using long-period grating refractometer. *Opt. Commun.* **2004**, *229*, 65–69. [[CrossRef](#)]
29. Liu, Y.; Qu, S. Femtosecond laser pulses induced ultra-long-period fiber gratings for simultaneous measurement of high temperature and refractive index. *Opt. Int. J. Light Electron Opt.* **2013**, *124*, 1303–1306. [[CrossRef](#)]
30. Liao, C.; Wang, Q.; Xu, L.; Liu, S.; He, J.; Zhao, J.; Li, Z.; Wang, Y. D-shaped fiber grating refractive index sensor induced by an ultrashort pulse laser. *Appl. Opt.* **2016**, *55*, 1525–1529. [[CrossRef](#)] [[PubMed](#)]
31. Venugopalan, T.; Sun, T.; Grattan, K.T.V. Temperature characterization of Long Period Gratings written in three different types of optical fibre for potential high temperature measurements. *Sens. Actuators A Phys.* **2010**, *160*, 29–34. [[CrossRef](#)]
32. Bai, Z.; Zhang, W.; Gao, S.; Zhang, H.; Wang, L.; Liu, F. Bend-insensitive long period fiber grating-based high temperature sensor. *Opt. Fiber Technol.* **2015**, *21*, 110–114. [[CrossRef](#)]
33. Deng, M.; Xu, J.; Zhang, Z.; Bai, Z.; Liu, S.; Wang, Y.; Zhang, Y.; Liao, C.; Jin, W.; Peng, G.; et al. Long period fiber grating based on periodically screw-type distortions for torsion sensing. *Opt. Express* **2017**, *25*, 14308–14316. [[CrossRef](#)] [[PubMed](#)]
34. Zhang, F.; Liu, S.; Wang, Y.; Huang, Y.; Xu, X.; Fu, C.; Wu, T.; Liao, C.; Wang, Y. Highly sensitive torsion sensor based on directional coupling in twisted photonic crystal fiber. *Appl. Phys. Express* **2018**, *11*, 042501. [[CrossRef](#)]
35. Liu, S.; Luo, M.; Ji, Q. Sensing Characteristics of Femtosecond Laser-Induced Long Period Gratings by Filling Cladding Holes in Photonic Crystal Fiber. *J. Lightwave Technol.* **2014**, *32*, 2287–2292.
36. Zhong, X.; Wang, Y.; Qu, J.; Liao, C.; Liu, S.; Tang, J.; Wang, Q.; Zhao, J.; Yang, K.; Li, Z. High-sensitivity strain sensor based on inflated long period fiber grating. *Opt. Lett.* **2014**, *39*, 5463–5466. [[CrossRef](#)] [[PubMed](#)]
37. Rao, Y.J.; Wang, Y.P.; Ran, Z.L.; Zhu, T. Novel fiber-optic sensors based on long-period fiber gratings written by high-frequency CO₂ laser pulses. *J. Lightwave Technol.* **2003**, *21*, 1320–1327.

